Nanomaterials and Nanosciences
ISSN 2053-0927

HOAJ
Herbert Open Access Journals

Research Open Access

Tunable resistive pulse sensing as a tool to monitor analyte induced particle aggregation

Emily R. Billinge[1], Julien Muzard[2] and Mark Platt[1*]
*Correspondence: m.platt@lboro.ac.uk
[1]Department of Chemistry, Centre for Analytical Science, Loughborough University, Loughborough, UK.
[2]Chaire de Bioinformatique, Conservatoire National des Arts et Metiers, Paris, France.

Abstract

Analytical technologies based upon superparamagnetic beads, SPBs, offer a rapid, simple and inexpensive way of separating and purifying the target analyte prior to detection. The SPBs can perform the capture, purification and the signal transduction stages, producing a simple, fast, and sensitive label-free format. Particle aggregation in the presence of the analyte is a common example of such a detection strategy. Herein we demonstrate the key parameters which lead to aggregation. We utilize a tunable resistive pulse sensing, TRPS, technology to follow the aggregation using three different methods of analysis. TPRS allows a comparison in the data treatment using average population values, particle concentration, and a more detailed analysis monitoring the change in aggregate size and frequency. To validate the approach, we use the well-known biotin-avidin binding assay to demonstrate the advantages and limitations of each type of analysis. Also presented are the key parameters that contribute to assay sensitivity such as bead concentration, size, binding capacities and data analysis.

Keywords: Superparamagnetic beads, resistive pulse sensing, aggregation, binding capacity

Introduction

The emergence of nano-materials and technology has catalyzed the search for new, low cost and robust detection and quantification methods. This research has been complemented and driven with the development, miniaturization and microfabrication of technologies available for point-of-care, *POC*, diagnostics and prognosis [1-5]. Detection strategies using nanomaterials are numerous and listed elsewhere in reviews [6] but can be generalized into spectroscopy [7-9], electrochemical [10,11] or magnetic [12].

Prior to analysis samples may require a pre-treatment stage involving purification or filtration to help ensure their compatibility with the technology platform. Superparamagnetic beads, SPBs provide an efficient and cost effective way to separate and pre-concentrate analytes from solution [13-16] helping to simplify and facilitate the front-end of an assay. They are readily available through numerous commercial sources and synthesis strategies [17], offering a range of surface chemistries that can be quickly conjugated to any capture probe of interest [13,18,19]. SPBs have demonstrated their versatility for use in conjunction with techniques such as the polymerase chain reaction [20] and mass spectroscopy [21], and have been utilized in high-throughput linear [13,22-25] and nonlinear magnetophoresis assays [14].

If the target analyte contains multiple epitopes, then it is possible for the target to bind to multiple beads simultaneously, leading to aggregation [13,26-29]. In such agglutination assays, the concentration of the analyte is inferred from the changes in aggregate size and/or frequency [30]. Using aggregation as an analytical signal allows for a simple "label-free" detection strategy and has been employed in conjugation with Au particles [31,32], fluorescence, or fluorescence resonance energy transfer [33] often in conjunction with optical, cytometry [34], magneto resistive sensing [35], and dynamic light scattering detection platforms [27,36]. Aggregation of SPBs does not typically result in a change in optical signal due to their optically dense iron oxide cores. Alternative detection strategies for monitoring aggregation using SPBs have relied upon light scattering techniques to monitor the size of the aggregates using chain length [36] or turbidity [27,37] and changes in magnetic properties as particles are forced to be in close proximity to each other [28]. These technologies have been demonstrated with detection levels down to picomolar levels, with assay times as low as 5 minutes, however light scattering and optical techniques can have a limited dynamic range and could prove difficult to multiplex [38].

The characterization of colloid and nanoparticle based systems has been aided in recent years by the resurgence and development of Coulter counting techniques such as micro- to nanopore based technologies [39-47]. Known collectively as resistive pulse sensing, *RPS*, they offer an attractive technology format because the measurements provide information on individual particles within their natural environment. RPS has been used to study numerous types of particles in different contexts with a very high resolution, including single molecules biophysics, protein sensing, biological detection [41,48,49] and synthetic nanoparticle characterization [47,50].

An elegant and novel adaptation to RPS using a tunable elastomeric pore technology, *TRPS* [46,49], allows for further versatility as the pore can be stretched in real time to suit the sample [50]. Techniques have been developed using TRPS to accurately determine the concentration [47], size and surface

doi: 10.7243/2053-0927-1-1

charge [51] of dispersed inorganic particles. TRPS is capable of detecting biological particles [44,49,52,53] as well as discriminating between particles of different surface chemistry and derivatives [29,54-56], and is typically used to measure particles with one dimension larger than 100 nm, making them suitable for a wide range of applications [46]. Recently we utilized a TRPS technology to monitor the aggregation of a special class of nanomaterial termed nanorods in the presence of analytes [29], other groups have monitored the aggregation of gold nanoparticles in the presence or absence of DNA to detect single nucleotide polymorphisms [57].

Whilst techniques have utilized the TRPS technology to monitor aggregation, the signal can often be complicated by particles traversing the pore in close proximity [56,58], and require beads with a uniform dimater. Here we present a comparison of the different strategies offered to interpret the aggregation signal using TRPS and have identified key parameters that control the aggregation of SPBs for the streptavidin-biotin assay, *i.e.,* bead concentration, bead size, binding capacity, reaction time, and application of magnetic force. The avidin-biotin interaction was used as a model as it is among the strongest known non-covalent specific molecular interactions, *i.e.,* $K_d \sim 10^{-15}$ M. Under the optimal assay conditions the assay could be used to detect aggregation in the presence of a biotinylated protein across five orders of magnitude. We also present results that correlate the concentration of analyte and the most stable and reproducible sizes of aggregates. We note that increases in the number of dimers for larger 3 micrometer beads best correlate with the increase in analyte concentration, whereas the smaller 300 nm particles form larger aggregates 8, 9 and 10mers in the presence of the analyte. This insight will help users optimize the TRPS setup for monitoring the aggregation signal, and offers an insight into the aggregation state of particles in the presence of the analyte.

Experimental

Materials

The particles used in this study were, Dynal particles carboxyl (1 micrometer - 650.12 and 3 micrometer -143.05D, Invitrogen UK), and Bio-Adembeads, 300 nm (2003233, Ademtech, Pessac, France). For the 3 micrometer beads 1mg = 5 x 10^7 beads, for the 1 micrometer beads 1mg = 6 x 10^8 beads, and the 300 nm beads 1mg = 1 x 10^{10} beads. Bovine serum albumin, BSA, 2-(N-Morpholino) ethanesulfonic acid (MES), Tween-20, and Sodium Dodecyl Sulphate (SDS) were all purchased from Sigma Aldrich (Gillingham, UK). 1 step ABTS solution, biotin-HRP, Biotin-BSA (BBSA), 1-Ethyl-3-(3-dimethylaminopropyl)carbodiimide hydrochloride (EDC), Sulfo-n-hydroxylsucciminide, *N*-hydroxysulfosuccinimide (sulfo-NHS) and avidin, were purchased from Thermo Scientific (Loughborough, UK). All chemicals and proteins were used as purchased without further purification. All particles were first collected with a magnet before being washed three times in the reaction buffer prior to use.

Buffers used

PBS (0.01 M phosphate buffer, 0.0027 M Potassium Chloride and 0.137 M Sodium Chloride, pH 7.4), PBST (PBS with 0.05 (v/v)% Tween). MES buffer (50 mM MES, pH 6.0). All separations were performed using a magnetic separator, "magrack 6" purchased from GE healthcare (Hatfield, UK).

Modification of the beads with avidin

Both the 1 and 3 micrometer diameter beads were modified with the avidin protein prior to the assay being performed. The beads (1 mg/ml) were washed three times with MES buffer, after the third wash step EDC (1 mg) and NHS (1 mg) were added to the solution in 1 ml of MES buffer, the particles were sonicated gently for 30 s and left on a rotating wheel allowing end-over-end mixing for 30 mins. This resulted in NHS activated beads. After 30 mins the particles were washed with MES buffer twice before a 1 ml PBS solution containing the required amount of avidin protein was added to the particles. The particles were sonicated gently for 30 s and left on a rotating wheel allowing end-over-end mixing for 3 hours. After this time the beads were washed with PBST three times before being resuspended in PBST containing 0.05% (wt/wt) BSA protein to block any nonspecific adsorption.

Protein coverage of beads

The binding capacities of all beads were measured using the standard biotin-HRP and ABTS quantification, the detailed procedure for which can be found elsewhere [59]. Briefy, 50 µl of beads (at 1 mg/ml) where washed with PBST once and incubated with a fresh PBST (0.05% wt/wt BSA) solution for 30 mins to block the surface and eliminate any non-specific adsorption. After 30 mins the beads were washed twice with PBST and incubated with 0.05 µg of Biotin-HRP protein in PBST for 30 mins. After 30 mins the beads were washed three times with PBST and resuspended in 100 µl of PBST. To this solution 200 µl of ABTS solution was added and the vial was placed onto a rotating wheel for 1 min. After 1 min 200 µl of 1% (wt/wt%) SDS "STOP" solution was added to the beads and the absorbance at 410 nm was recorded. This final absorbance value was converted into a binding capacity using a calibration curve (standards) of known biotin-HRP protein.

Assay format

The SPBs (1 mg/ml) were routinely stored in PBST buffer containing 0.05 (wt/wt%) BSA. This storage served to act as a blocking solution reducing non-specific adsorption. When required the SPBs were diluted to the required concentration, and sonicated briefly (<10 s). Typical assay volumes were ~500 – 1000 µl. The final dilution of the beads and its resultant concentration is reported in all graphs and calculations. Samples were prepared by diluting the target BBSA into PBST. The solution was incubated at room temperature on

 doi: 10.7243/2053-0927-1-1

a rotating wheel allowing end-over-end mixing. After the required hybridization time, the sample was either analyzed immediately, or subject to the magnetic assisted aggregation. Each experiment was run multiple times and the standard deviation of each point is displayed in the errors bars on the graphs.

Magnetic assisted aggregation, MAS

For the assisted aggregation - the sample was placed next to a permanent magnet, until all the beads were judged to have come out of solution after ~ 1 min. The magnet had a field strength of 1 mT present up to 6 mm from the neodymium magnet bar on its surface. The initial solution was removed leaving all the beads on the side of the container and 500 µl PBS was added to the beads. The solution was stirred and the magnet was replaced separating the beads for a second time. When required the magnet was replaced for a third and fourth time. During the last separation, the magnet was removed allowing the pellet to settle to the bottom of the vial for 30 s before finally being vortexed ensuring the beads were evenly dispersed in the solution for analysis. This process aims at increasing the number of particle-particle interactions and thus increase the number of particle aggregates.

Effects of adding additional particles to the reaction after the MAS

During the magnetic assisted aggregation process described above, after the first MAS the analyte solution was removed and an additional 500 µl solution of beads in PBST was added to the sample vial. The aliquot contained the same concentration of beads as the original solution, thus doubling the concentration of beads. They were then treated with the same method described above.

TRPS setup

Measurements were made using the qNano system obtained from Izon Science (Christchurch), which incorporates the fluid cell, stretching apparatus, data recording and analysis software (v.2.2) and the pore specimens themselves [**46**,**47**]. The pores used were designated 'NP4000' for use with the 3 micrometer beads and most suitable, as determined by the manufacturer, for detecting particles in the range 2000 – 8000 nm, 'NP1000' for use with the 1 micrometer beads and most suitable for detecting particles in the range 500 – 2000 nm and 'NP400' for use with the 300 nm beads and most suitable for detecting particles in the range 200 – 800 nm. The tunable pores can be reused and in each set of experiments only one pore for each size of particle was needed. A typical setup for each membrane was: NP4000, Stretch 3.5 mm, Voltage 0.04V; NP1000, Stretch 5 mm, Voltage 0.04V; NP400, Stretch 5 mm, Voltage 0.32V [**29**]. Once a baseline current of approx. 100 nA ± 10 was established for each membrane the potential and stretch were kept constant during the experiment *i.e.,* it never changed during the data capture or changed between each sample. Once the instrument was setup under the above conditions, it was stable over a period of hours. After each sample was analysed only the upper fluid cell needed to be washed with PBST to ensure no residual particles remained and the membrane stability meant that it did not need to be relaxed after each measurement. To further verify the upper cell was clean of residual aggregates, a PBST solution was placed into the cell and the signal recorded for 2 mins to ensure a stable baseline with no pulses observed. Izons calibration beads (obtained with the instrument) were used to calculate the initial concentration and size of all the particles, particles 955 nm in diameter, and 350 nm in diameter were used for this purpose.

Data analysis

Each particle that traverses the pore is recorded as a pulse event, termed Δi_p, the magnitude of the pulse or peak magnitude, can be related to the particle size, and their frequency used to determine the concentrations. Data capture was performed using Izon's control suite 2.2 software. The number of data points captured for each experiment exceeded 500. In all measurements a noise threshold of 0.1 nA was used and all recorded events were clearly distinguishable from this noise level in the baseline current.

During the first step of the assay, avidin functionalized SPBs were added to a solution containing biotinylated-BSA, each BSA protein contains an average of 9 biotin molecules per BSA protein (data from supplier). The solution was incubated on a rotating wheel for 25 minutes and in the second step, an external magnetic gradient was applied to the bead suspensions to separate the beads and accelerate the rate of bead interaction with each other, in all experiments unless stated the number of MAS stages was always two. In the final step a 40 microlitres aliquot of the sample was placed into the TRPS technology for analysis. During the incubation period the instrument was setup as described above, a stable baseline current was established prior to running the samples. When required calibration beads were passed through the pore at the start and at the end of each experiment to allow the concentration and size of the beads to be determined.

Method 1: Average size

Upon processing the raw data with the software a ".txt" file was created which contained information on each pulse recorded during the experiment. The peak height and time was extracted from the data and copied into a spreadsheet. Further analysis of the data was carried out using Microsoft Excel 2010. The average peak height was calculated from all the data points captured and plotted against concentration.

Method 2: Determining the change in bead concentration

The initial concentration of beads was calculated using the calibration beads. During each experiment a "blank" sample, a solution containing no analyte, was then used as a calibration

doi: 10.7243/2053-0927-1-1

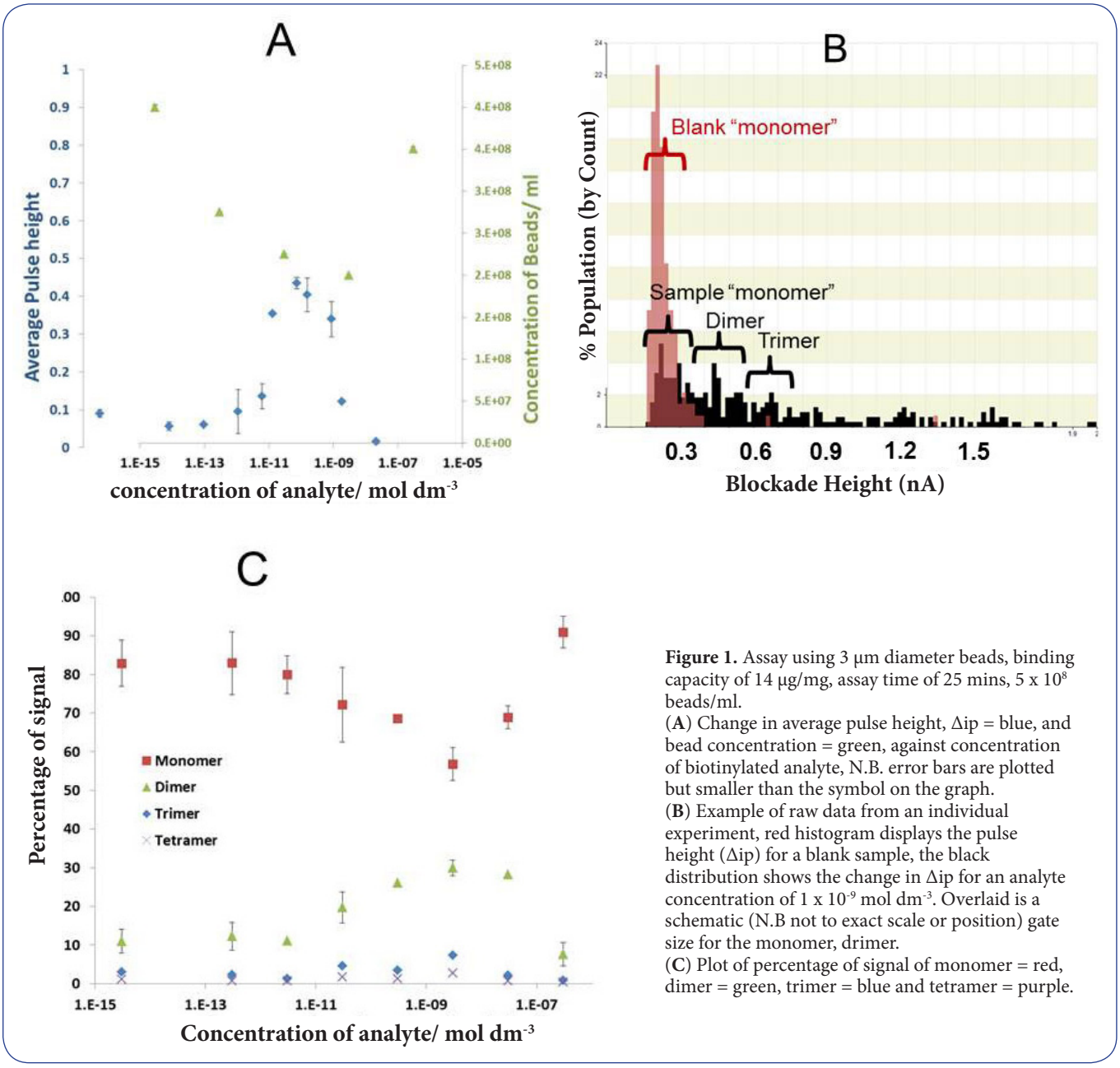

Figure 1. Assay using 3 μm diameter beads, binding capacity of 14 μg/mg, assay time of 25 mins, 5 x 10^8 beads/ml.
(**A**) Change in average pulse height, Δip = blue, and bead concentration = green, against concentration of biotinylated analyte, N.B. error bars are plotted but smaller than the symbol on the graph.
(**B**) Example of raw data from an individual experiment, red histogram displays the pulse height (Δip) for a blank sample, the black distribution shows the change in Δip for an analyte concentration of 1 x 10^{-9} mol dm^{-3}. Overlaid is a schematic (N.B not to exact scale or position) gate size for the monomer, drimer.
(**C**) Plot of percentage of signal of monomer = red, dimer = green, trimer = blue and tetramer = purple.

file for the remaining experiments. To monitor the changes in bead concentration as a function of the analyte concentration, each subsequent sample was then compared against the concentration of beads in the "blank" file.

Method 3: Monitoring the change in aggregate size

The data was extracted as a .txt file as described above. The blank sample described above was used to determine the location and size of the monomer and larger aggregate peaks. As the blank sample contained no analyte and therefore the observed signal represented monomers, a bin size which accounted for these data points was determined. The bin size ranged from the lowest peak current, lpc, upto 94% of the max peak current, mpc, observed for the monomers. A value of 94% was chosen to omit the slight tail in the data set seen in **Figure 1B**. As the peak height is proportional to the volume displaced by the traversing particle [**44**,**47**] a dimer would produce twice the signal and therefore any signal that was observed within 0.94mpc + (0.94mpc–lpc) was counted as a dimer, thus every subsequent window was simply an increase of (0.94mpc–lpc). A histogram could then be constructed using multiples of the monomer peak to determine the number of larger aggregates. Once the number of data points for each bin had been calculated from the raw data, the number was

 doi: 10.7243/2053-0927-1-1

converted into a percentage by dividing it by the total number of data points for the experiment. The ratio was then plotted as a function of analyte concentration. In each experiment the fraction of aggregates up to and including the 12mers was calculated, even if they are not plotted in the figures. All experiments were repeated at least once and in some cases triplicate, where error bars are shown they represent the standard deviation around the mean value taken from at least triplicate repeat experiments.

Results and discussion

Comparing methods for analyzing the aggregation of beads

Method 1: The simplest way to analyze the data, is to plot the mean peak size, Δi_p, signal versus analyte concentration, as shown in **Figure 1A** (blue diamonds). As the concentration of the analyte is increased the average Δi_p remains steady until a sharp increase around 1 x 10^{-9} mol dm^{-3} of analyte. The mean pulse height continues to increase up to an analyte concentration of 1 x 10^{-8} mol dm^{-3} before decreasing back to its original value. The increase in Δi_p can be attributed to the particles forming larger aggregates in the presence of the analyte, at lower concentrations of analyte the number of aggregates is too low to be detected as the majority of the signal comes from the individual monomers. The decrease in signal from aggregation at high concentrations of analytes has been well documented for agglutination assays. It results from the saturation of the binding sites on the particle surface with the analyte and is known as the 'hook' effect. Plotting the mean Δi_p as a function of concentration seems insensitive to analyte concentrations below 1 x 10^{-9} mol dm^{-3}.
Method 2: An alternative method is to follow the change in particle concentration. The TRPS method can be calibrated to calculate the concentration of the particles, as the flux, *J*, of particles through the pores is directly proportional to their concentration [**44**]. As the particles aggregate the total number of beads in solution decreases, as monomers are consumed into growing particle clusters. The TRPS technology was calibrated to measure the change in particle concentration. The same data used for the above Δi_p measurements was re-analyzed, the results are plotted in **Figure 1A** (green triangles). Measuring the change in bead concentration seems to be more sensitive, and a decrease in bead count can be observed at concentrations as low as 1 x 10^{-12} mol dm^{-3}. However with this method the measured bead concentrations varied in repeat runs by up to 45%, shown in **Supplement figure S1** As a comparison the triplicate measurements for methods 1 are shown in **Supplement figure S2**. If insufficient time is given for the beads to come out of solution in the presence of the magnet, or beads are washed out of the vial during the MAS stage the variation from run to run may be effected. Therefore, if the technique is to be used across multiple labs the variation in the technician's patience in waiting for all the beads to be extracted from the solution could leads to variations in the results. Given that we hope to develop this technique for the detection of analytes, the user reproducibility must be high, and a more robust method of data analysis is needed.

In this study commercial Dynal and Ademtech beads with relatively uniform diameters, <2% and <10% CV, respectively, were used. When the SPBs are highly uniform in diameter, it is possible to isolate the signal from the larger aggregates from that of the individual beads. Method 3: **Figure 1B** shows the raw data from the Izon software for the "Blank/Background" (red) and a "Sample" exposed to the analyte (black). In the blank sample the beads produce an individual peak which we term "monomers". The gate was titled "monomer", as the Δi_p is proportional to volume of the particle traversing the pore, a dimer should have twice the signal of a monomer. Therefore, by doubling the gate size the number of dimers could be counted. A similar process can be done to account for the trimers, tetramers etc. **Figure 1C** summarizes the quantitative analysis of the percentage of monomers, dimers, trimers and tetramers formed in the assay using the 3 micrometer beads, as a function of analyte concentration. At concentrations between 10^{-12} and 10^{-9} M there was a direct correlation between the number of dimer aggregates and the analyte concentration, $R^2 = 0.936$. Again at concentrations greater than 1 nM there was a decrease in number of all sizes of aggregates and increase in monomers was observed due to the onset of the hook effect. The variation in results, from assay to assay was lower using this analysis, the average coefficient of variation for data points across the entire concentration was no more than 25%, whereas for methods one and two the CV range which from 35-65%. The reasons being 1 – that the average population value is no longer being used, and therefore the small number of larger aggregates is not lost on the analysis, and 2 – we use the fraction of the beads that are remaining, if any particles are lost during the wash and MAS stages it does not impact upon the ratio between monomers and larger aggregates. The assumption would be that we lose an equal proportion of monomers and dimers during any washing steps which may not hold true as larger aggregates tend to separate out from solution at faster rates. However the reduction in errors bars and the mirroring of the dimer and monomer peak suggest that we do not have a strong sample bias. We therefore continued to use this method to monitor particle aggregation.

Influence of magnetic assisted aggregation, MAS, on the hook effect

Figure 2A presents the number of monomers as a function of analyte concentration and number of MAS performed. The influence of magnetic extraction on the assay itself was determined by analyzing the number of monomers with and without the MAS. Several observations can be made from these results, firstly in the absence of the MAS (green triangles) fewer aggregates appear to form, and the number of monomers is high across the range of analyte concentrations. In the absence

doi: 10.7243/2053-0927-1-1

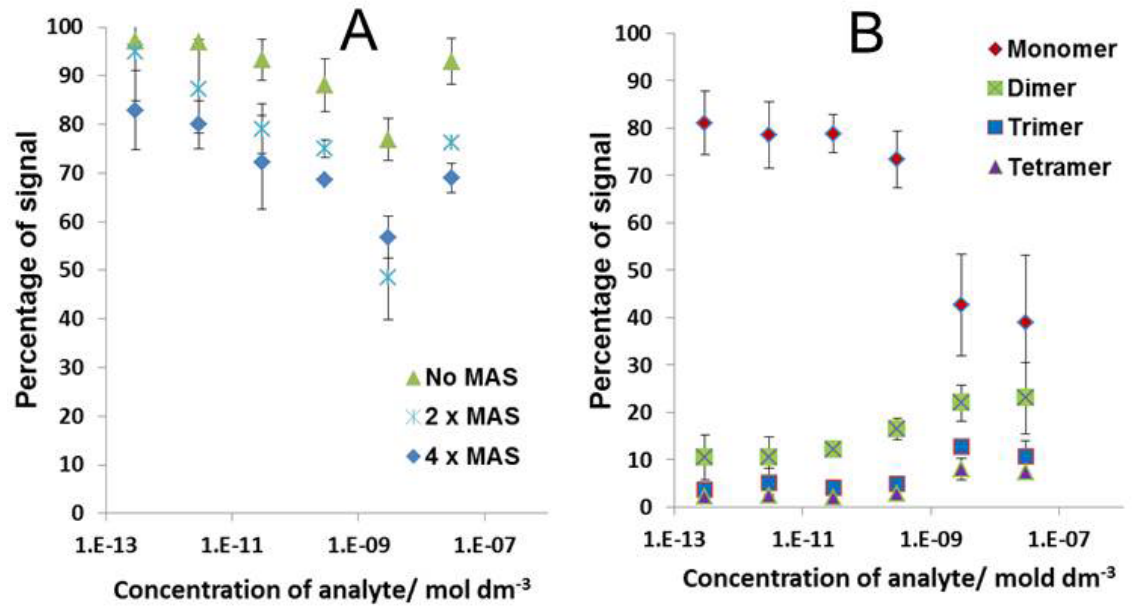

Figure 2. (**A**) Effect of the number of MAS on the distribution of monomers for the reaction conditions using 5 x 10^8 beads / ml of 3 μm avidin modified beads 25 min assay time, binding capacity 14 μg/mg. (**B**) Under the same bead conditions as A, Effect of the addition of new beads during the MAS. red = monomer, green = dimer, blue = trimer and purple = tetramer.

of the MAS bringing the beads together, aggregates are only formed if two beads collide in solution with the correct orientation and alignment to form a bond. Upon the addition of the magnetic field the number of interactions increases, leading to an increase in aggregation and the decrease in the number of monomers. Increasing the number of MAS stages from 2 to 4 does not seem to drastically decrease the number of monomers across the concentration range and allows the user to pick the most convenient number for their assay conditions and time allowances.

The hook effect could be problematic during an analytical measurement as two concentrations of analyte in solution could in theory produce the same aggregation ratio. To explore the possibility of removing the hook effect, we added a second aliquot of beads to the solution after the first MAS stage. The MAS stage was repeated two more times and the sample analyzed. **Figure 2B** displays the results and the fraction of the sample that was measured to be mono, di, tri and tetramers. It is evident from **Figure 2B** that the characteristic decrease in aggregate signal and increase in monomer signal typically observed at high concentrations of analyte in previous experiments has been shifted beyond the concentration range being measured here, and a gradual decrease in monomer signal is observed across the entire range of the assay. The explanation for this is that at high concentrations of analyte the majority of the binding sites on the beads are occupied. Therefore when brought into contact with each other no free binding sites are available to form aggregates. The addition of fresh beads after the first MAS stage introduces vacant binding sites leading to aggregation.

Influence of binding capacity, concentration, and diameter

To further investigate the onset of aggregation and dynamic range of the assay, a set of experiments was devised in which the binding capacity was systematically varied. **Figure 3A** and **3B** present the percentage of monomers and dimers, respectively, produced by the reaction of 3 micrometer SPBs across a range of analyte concentrations. In each experiment the binding capacity of the beads was gradually decreased from 14 μg/mg to 3 μg/mg. As the binding capacity was lowered, the magnitude of the change in the numbers of monomers and dimers, decreases. Hence as the binding capacity is reduced the beads are less efficient at forming aggregates and therefore the signal is diminished.

Figure 4A illustrates the effect of lowering the number of beads in the assay, and thus reducing the total number of binding sites. This has the effect of shifting the onset of the hook effect to a lower concentration. Whilst the hook effect appears at a lower analyte concentration it is also worth noting that a greater decrease in monomer signal is also observed changing from 70% for the 2.5 × 10^8 beads/ml down to 40% of the signal for the 1 × 10^7 beads/ml, effectively making the onset of aggregation easier to observe. The onset of the hook effect was found to be closely linked to both the concentration of avidin in the reaction and the density of avidin on the beads. To test the effect of particle size a similar set of experiments were then performed with biotinylated-BSA

doi: 10.7243/2053-0927-1-1

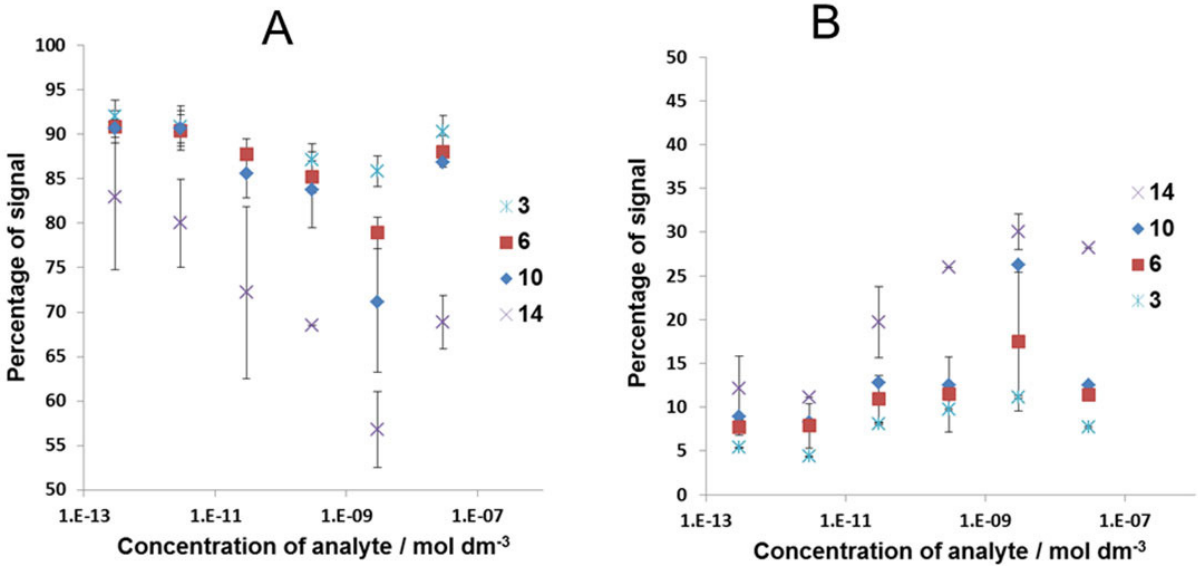

Figure 3. Distribution of monomers (**A**), and dimers (**B**), for the reaction conditions using 5 x 10^8 beads /ml of 3 μm avidin modified beads. The binding capacity, displayed in the legend in terms of μg/mg of beads was varied and the intensity of change in aggregate size plotted as a function of analyte concentration.

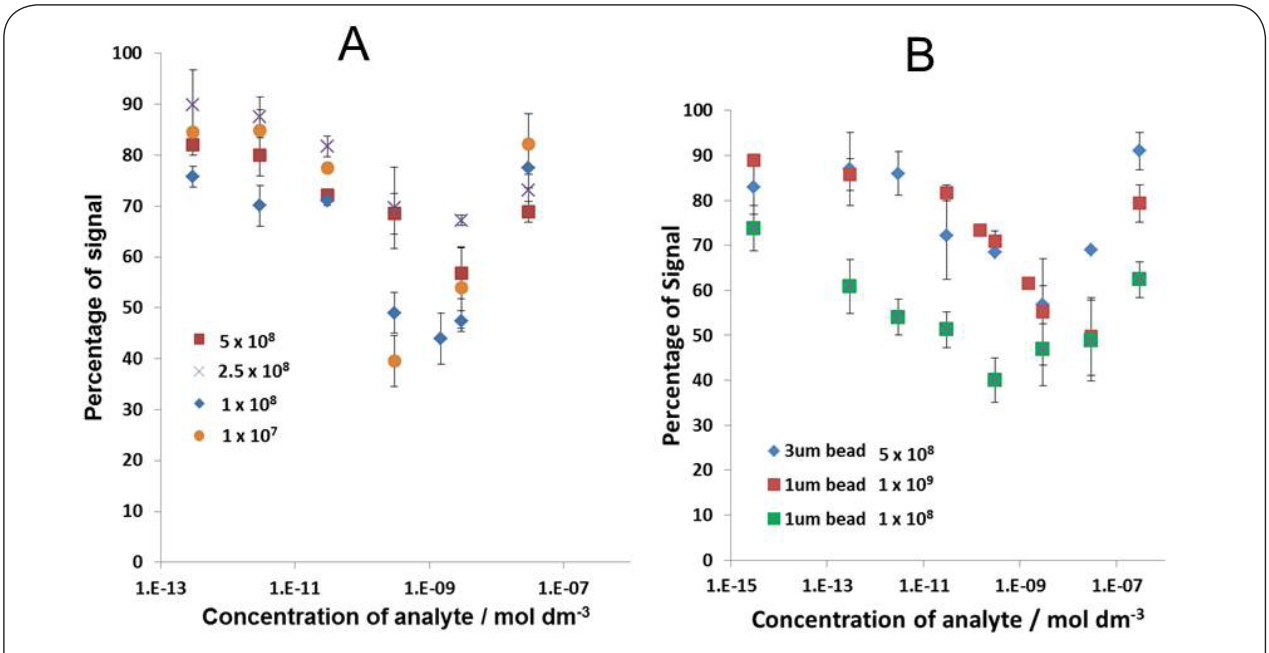

Figure 4. (**A**) Effect of concentration of beads upon maximum decrease in monomer signal using 3 μm avidin modified beads, binding capacity of 14 μg/mg, 25 min assay time and 5 x 10^8 beads /ml = red, 2.5 x 10^8 beads /ml = purple, 1 x 10^8 beads /ml = blue an 1 x 10^7 beads /ml = orange. Highlighted on the graph is the minimum in each curve for the dilutions. (**B**) Effect of concentration of beads upon maximum decrease in monomer signal, 25 min assay: 3 μm avidin modified beads 5 x 10^8 beads /ml, binding capacity 14 μg/mg = blue, 1 μm avidin modified beads, 6 x 10^9 beads /ml, binding capacity 20 μg/mg = red, and 1 μm avidin modified beads, 5 x 10^8 beads /ml binding capacity 20 μg/mg = green.

for avidin functionalized 1 micrometer beads and the results are shown in **Figure 4B**. Qualitatively similar trends were observed, *i.e.,* both the intensity and position of the maximum number of aggregates can be tailored by changing the bead number and binding capacity. Quantitatively, however, the results for the 1 micrometer beads differed from the 3 micrometer beads. It is clear from **Figure 4B** that when a similar concentration of beads are used (green and blue)

doi: 10.7243/2053-0927-1-1

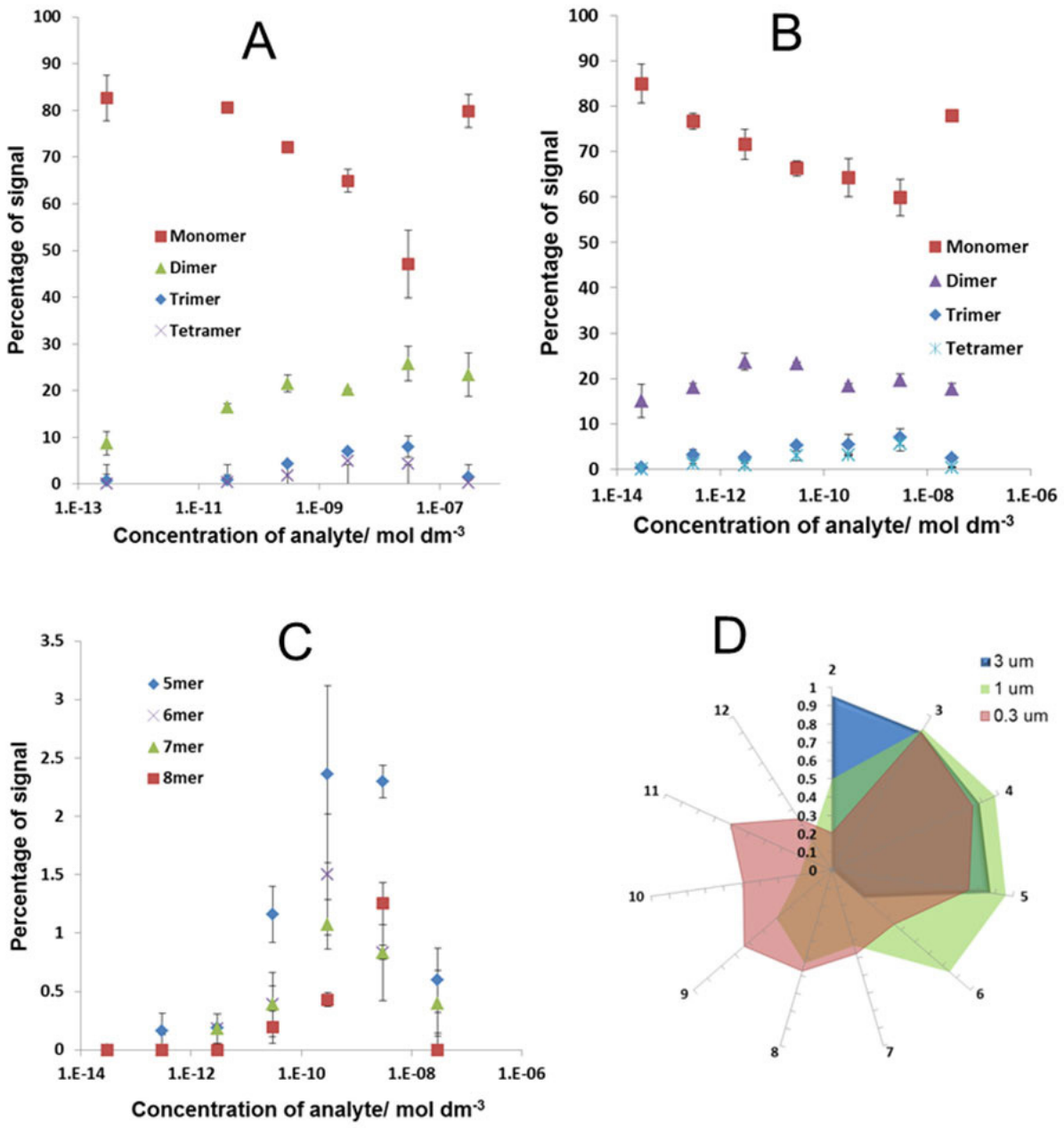

Figure 5. (**A**) Distribution of monomer = red, dimer = green, trimer = blue and tetramer = purple. 1 µm avidin modified beads 25 min assay time 6 x 10^9 beads /ml, binding capacity 20 µg/mg. (**B**) Distribution of monomer = red, dimer = green, and tetramer = purple using 0.3 µm Streptavidin modified beads 25 min assay time 1 x 10^{10} beads /ml, binding capacity 4 µg/mg. (**C**) Distribution of 5mer = blue, 6mer = purple, and 7mer = green and 8mer = red using 0.3 µm Streptavidin modified beads 25 min assay time 1 x 10^{10} beads /ml binding capacity 4 µg/mg. (**D**) Correlation, R^2 value, plotted along the axis between the increase in aggregate size versus the decrease in monomer signal for the three different bead sizes.

the peak in aggregation appeared at a lower concentration of analyte for the 1 micrometer beads, and a larger fraction of beads formed aggregates. The interpretation of this result is that when the same number of 1 and 3 micrometer beads are used the 1 micrometer beads aggregate more efficiently. This is most likely due to the fact that the 1 micrometer beads have a higher rotational diffusion coefficient. When the total binding capacity of the 1 micrometer beads was increased to 20 µg/mg *i.e.,* more 1 micrometer beads were added to solution (blue and red) the onset of the hook effect again is shifted to a higher concentration of analyte, reflecting the change in total binding capacity of the beads surface.

The change in behavior from lowering the binding capacity of the beads – **Figure 3**, and changing the total number of

doi: 10.7243/2053-0927-1-1

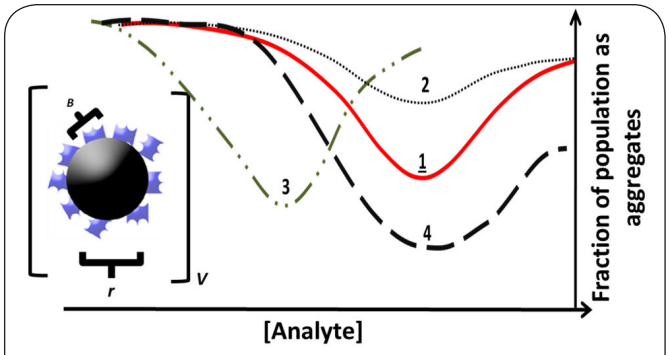

Figure 6. Schematic of the changes in monomer population related to physical properties of the SPBs. 1 – Reference curve. 2 - Decrease binding capacity, B. 3 – Decrease concentration, V. 4 – Decrease bead diameter, r.

beads in solution - **Figure 4**, relates to change in the rate of reactions and efficiencies at forming the aggregates [**27**,**60**]. As we change the number of beads in solution, we can shift the onset of the hook effect by simply changing the total binding capacity, **Figure 4**. As we keep the same numbers of beads in solution but alter the number of binding sites per bead, the probability of the bead and analyte colliding and forming a bond decreases, as the reaction rate is proportional to the surface coverage of streptavidin [**30**]. When the number of free binding sites decreases the number of collisions that result in the successful capture of the analyte or aggregate decreases and as opposed to see a shift in the hook effect we see the aggregation signal decrease.

Whilst performing the aggregation assays we noted that the sizes of aggregates for the 1 micrometer beads when compared to the 3 micrometer beads where typically larger, *i.e.,* larger numbers of gates were required to count all the data points **Figure 5A**. As we used a different pore size for each particle set, we cannot say with absolute certainty that the different pores would discriminate against larger aggregates, and the following observations and discussion are made based upon the assumption that we observe the majority of the signal from the particles and aggregates, in addition we use beads from two suppliers which may differ in physical properties.

To investigate the relationship between bead size and aggregate size a smaller 300 nm bead functionalized with streptavidin was added to the target analyte. A comparable binding capacity was used; the results of the assay are shown in **Figures 5B** and **5C**. In **Figure 5B** the change in monomers, dimers trimmers and tetramers are plotted as a function of analyte concentration, a similar trend in monomer concentration is observed and the numbers of monomers decrease as the analyte concentration increases. Unlike the larger 3 micrometer particles the increase in the number of dimers in **Figure 5B**, shows no correlation with the monomers, $R^2 = 0.2$, and it appears that the larger tetramers mirror the monomer relationship. **Figure 5C** plots the larger 5,6,7 and 8 mers versus concentration and whilst their signal intensity is weak they show some correlation with the monomer trend. We plotted the correlation between the decrease in monomers and the number of larger aggregates measured for the 3, and 0.3 micrometer diameter beads as illustrated in **Figure 5D**. For the larger 3 micrometer beads we observe a strong correlation between the decrease in monomers and the increase in 2-4mers in solution, $R^2 \sim 0.9$. As the beads diameter decreases the correlation between the number of monomers decreasing and the increase in dimers reduces from R^2 - 0.96 to 0.5 and 0.2 for the 3, 1 and 0.3 micrometer beads respectively. With the smaller 0.3 micrometer particles we see a correlation between the increase in 3-5mers and 9-11mers with the decrease in monomer concentration. The smaller particles seem to form larger and more readily measurable aggregates, and one possible explanation is that the smaller beads have an ability to nucleate and grow in aggregate size, mimicking crystallization of nanoparticles. Micron sized particles have previously been used as model systems to aid with nucleation and growth studies [**61**-**63**]. Similar observations of cluster size might have proven difficult using flow cytometry or light scattering techniques and the TRPS may offer the possibility of studying the aggregation and growth of colloidal particles in solution.

Conclusions

In the current study, we have used TRPS technology to characterize the aggregation state of avidin functionalized particles in the presence of a biotinylated target. We have attempted to present several methods of data interpretation, aimed at increasing the reproducibility of the experiment and allowing for a detailed and informative study of the aggregation state. We have then used the TRPS technology to investigate the key experimental variables in designing a magnetic aggregation assay. A summary of all the factors that were found to influence the onset of aggregation can be found in **Figure 6**. The resulting assay platform was capable of operating over several orders of magnitude of concentration; the ability to measure aggregation can be improved by increasing the density of receptors on the beads, decreasing the size of the beads used, and/or decreasing the total number of beads used in the assay. However, lowering binding capacity and bead number resulted in a more rapid saturation of the beads with analyte and thus the hook effect appeared at lower analyte concentrations. By controlling the particle size, binding capacity, and particle concentration, the aggregation of SPBs in the presence of the target analyte can be tailored and predicted to produce a simple and sensitive analytical method.

Additional files

Supplement figure S1
Supplement figure S2

Competing interests

The authors declare that they have no competing interests.

doi: 10.7243/2053-0927-1-1

Authors' contributions

Emily Billinge performed experiments, prepared the manuscript and provided scientific input. Julien Muzard provided scientific advice, supporting in designing the experiments and writing the manuscript. Mark Platt performed the experiments, designed the experiments wrote the document, performed the preliminarily data analysis and managed the project.

Acknowledgement

The authors thank D. Aubert, C. Williams and H. Van der Voorn for support. The members of the Bionanoscience group at University College Dublin for their intellectually stimulating discussion and S. G. Platt for his inspiration and motivation. Funding was provided by the European Commission for Research (PCIG11-GA-2012-321836 Nano4Bio), and Loughborough University Chemistry Department (Start up fund).

Publication history

Editor: Fadong Yan, College of Nanoscale Science and Engineering, USA.
Received: 25-Mar-2013 Revised: 02-May-2013
Re-Revised: 03-Jun-2013 Accepted: 04-Jun-2013
Published: 14-Jun-2013

References

1. RSC and Publishing, **Analysis for Healthcare Diagnostics and Theranostics.** *Faraday Discussion 149* 2010. | Website
2. Myers FB and Lee LP: **Innovations in optical microfluidic technologies for point-of-care diagnostics**. *Lab Chip* 2008, **8**:2015-31. | Article | PubMed
3. Weigl B, Domingo G, Labarre P and Gerlach J: **Towards non- and minimally instrumented, microfluidics-based diagnostic devices**. *Lab Chip* 2008, **8**:1999-2014. | Article | PubMed Abstract | PubMed Full Text
4. Frost & Sullivan: **Advances in Point-Of-Care technologies**. *Technical Insights* D133. | Website
5. Rowe W, Platt M and Day PJ: **Advances and perspectives in aptamer arrays**. *Integr Biol (Camb)* 2009, **1**:53-8. | Article | PubMed
6. Rosi NL and Mirkin CA: **Nanostructures in biodiagnostics**. *Chem Rev* 2005, **105**:1547-62. | Article | PubMed
7. Elghanian R, Storhoff JJ, Mucic RC, Letsinger RL and Mirkin CA: **Selective colorimetric detection of polynucleotides based on the distance-dependent optical properties of gold nanoparticles**. *Science* 1997, **277**:1078-81. | Article | PubMed
8. Storhoff JJ, Elghanian R, Mucic RC, Mirkin CA, and Letsinger RL: **One-Pot Colorimetric Differentiation of Polynucleotides with Single Base Imperfections Using Gold Nanoparticle Probes**. *Journal of the American Chemical Society* 1998, **120**(9):1959-1964. | Article
9. Reynolds RA, Mirkin CA, & Letsinger RL: **Homogeneous, Nanoparticle-Based Quantitative Colorimetric Detection of Oligonucleotides**. *Journal of the American Chemical Society* 2000, **122**(15):3795-3796. | Article
10. Park SJ, Taton TA and Mirkin CA: **Array-based electrical detection of DNA with nanoparticle probes**. *Science* 2002, **295**:1503-6. | Article | PubMed
11. Weizmann Y, Patolsky F and Willner I: **Amplified detection of DNA and analysis of single-base mismatches by the catalyzed deposition of gold on Au-nanoparticles**. *Analyst* 2001, **126**:1502-4. | Article | PubMed
12. Perez JM, Josephson L, O'Loughlin T, Hogemann D and Weissleder R: **Magnetic relaxation switches capable of sensing molecular interactions**. *Nat Biotechnol* 2002, **20**:816-20. | Article | PubMed
13. Chang WS, Shang H, Perera RM, Lok SM, Sedlak D, Kuhn RJ and Lee GU: **Rapid detection of dengue virus in serum using magnetic separation and fluorescence detection**. *Analyst* 2008, **133**:233-40. | Article | PubMed
14. Yellen BB, Erb RM, Son HS, Hewlin R, Jr., Shang H and Lee GU: **Traveling wave magnetophoresis for high resolution chip based separations**. *Lab Chip* 2007, **7**:1681-8. | Article | PubMed
15. Prodelalova J, Rittich B, Spanova A, Petrova K and Benes MJ: **Isolation of genomic DNA using magnetic cobalt ferrite and silica particles**. *J Chromatogr A* 2004, **1056**:43-8. | Article | PubMed
16. Kang K, Choi J, Nam JH, Lee SC, Kim KJ, Lee SW and Chang JH: **Preparation and characterization of chemically functionalized silica-coated magnetic nanoparticles as a DNA separator**. *J Phys Chem B* 2009, **113**:536-43. | Article | PubMed
17. Sandhu A, Handa H and Abe M: **Synthesis and applications of magnetic nanoparticles for biorecognition and point of care medical diagnostics**. *Nanotechnology* 2010, **21**:442001. | Article | PubMed
18. Llandro J, Palfreyman JJ, Ionescu A and Barnes CH: **Magnetic biosensor technologies for medical applications: a review**. *Med Biol Eng Comput* 2010, **48**:977-98. | Article | PubMed
19. Latham AH and Williams ME: **Controlling transport and chemical functionality of magnetic nanoparticles**. *Acc Chem Res* 2008, **41**:411-20. | Article | PubMed
20. Kojima T, Takei Y, Ohtsuka M, Kawarasaki Y, Yamane T and Nakano H: **PCR amplification from single DNA molecules on magnetic beads in emulsion: application for high-throughput screening of transcription factor targets**. *Nucleic Acids Res* 2005, **33**:e150. | Article | PubMed Abstract | PubMed Full Text
21. Whiteaker JR, Zhao L, Zhang HY, Feng LC, Piening BD, Anderson L and Paulovich AG: **Antibody-based enrichment of peptides on magnetic beads for mass-spectrometry-based quantification of serum biomarkers**. *Anal Biochem* 2007, **362**:44-54. | Article | PubMed Abstract | PubMed Full Text
22. Beveridge JS, Stephens JR, Latham AH and Williams ME: **Differential magnetic catch and release: analysis and separation of magnetic nanoparticles**. *Anal Chem* 2009, **81**:9618-24. | Article | PubMed
23. Pamme N: **Continuous flow separations in microfluidic devices**. *Lab Chip* 2007, **7**:1644-59. | Article | PubMed
24. Pamme N and Wilhelm C: **Continuous sorting of magnetic cells via on-chip free-flow magnetophoresis**. *Lab Chip* 2006, **6**:974-80. | Article | PubMed
25. Afshar R, Moser Y, Lehnert T and Gijs MA: **Three-dimensional magnetic focusing of superparamagnetic beads for on-chip agglutination assays**. *Anal Chem* 2011, **83**:1022-9. | Article | PubMed
26. Park SY, Ko PJ, Handa H, & Sandhu A: **Exploring magneto-optical properties of biofunctionalized magnetic chains for developing label-free immunoassays**. *Journal of Applied Physics* 2010, 107(9):09B324-323. | Article
27. Baudry J, Rouzeau C, Goubault C, Robic C, Cohen-Tannoudji L, Koenig A, Bertrand E and Bibette J: **Acceleration of the recognition rate between grafted ligands and receptors with magnetic forces**. *Proc Natl Acad Sci U S A* 2006, **103**:16076-8. | Article | PubMed Abstract | PubMed Full Text
28. Koh I, Hong R, Weissleder R and Josephson L: **Nanoparticle-target interactions parallel antibody-protein interactions**. *Anal Chem* 2009, **81**:3618-22. | Article | PubMed Abstract | PubMed Full Text
29. Platt M, Willmott GR and Lee GU: **Resistive pulse sensing of analyte-induced multicomponent rod aggregation using tunable pores**. *Small* 2012, **8**:2436-44. | Article | PubMed
30. Gubala V, Lynam CC, Nooney R, Hearty S, McDonnell B, Heydon K, O'Kennedy R, MacCraith BD and Williams DE: **Kinetics of immunoassays with particles as labels: effect of antibody coupling using dendrimers as linkers**. *Analyst* 2011, **136**:2533-41. | Article | PubMed
31. Huang CC, Huang YF, Cao Z, Tan W and Chang HT: **Aptamer-modified gold nanoparticles for colorimetric determination of platelet-derived growth factors and their receptors**. *Anal Chem* 2005, **77**:5735-41. | Article | PubMed
32. Chang JY, Wu H, Chen H, Ling YC and Tan W: **Oriented assembly of Au nanorods using biorecognition system**. *Chem Commun (Camb)* 2005, 1092-4. | Article | PubMed
33. Pollitt SK, Pallos J, Shao J, Desai UA, Ma AA, Thompson LM, Marsh JL and Diamond MI: **A rapid cellular FRET assay of polyglutamine aggregation identifies a novel inhibitor**. *Neuron* 2003, **40**:685-94. | Article | PubMed
34. Arndt PA and Garratty G: **A critical review of published methods for analysis of red cell antigen-antibody reactions by flow cytometry, and approaches for resolving problems with red cell agglutination**. *Transfus*

Med Rev 2010, **24**:172-94. | Article | PubMed

35. Ranzoni A, Schleipen JJ, van Ijzendoorn LJ and Prins MW: **Frequency-selective rotation of two-particle nanoactuators for rapid and sensitive detection of biomolecules**. *Nano Lett* 2011, **11**:2017-22. | Article | PubMed
36. Park SY, Handa H and Sandhu A: **Magneto-optical biosensing platform based on light scattering from self-assembled chains of functionalized rotating magnetic beads**. *Nano Lett* 2010, **10**:446-51. | Article | PubMed
37. Ranzoni A, Schleipen JJ, van Ijzendoorn LJ and Prins MW: **Frequency-selective rotation of two-particle nanoactuators for rapid and sensitive detection of biomolecules**. *Nano Lett* 2011, **11**:2017-22. | Article | PubMed
38. Anderson W, Kozak D, Coleman VA, Jämting ÅK, & Trau M: **A comparative study of submicron particle sizing platforms: Accuracy, precision and resolution analysis of polydisperse particle size distributions**. *Journal of Colloid and Interface Science* 2013. | Article
39. Lan W-J, Holden DA, Liu J, & White HS: **Pressure-Driven Nanoparticle Transport across Glass Membranes Containing a Conical-Shaped Nanopore**. *The Journal of Physical Chemistry C* 2011, **115**(38):18445-18452. | Article
40. Lan WJ, Holden DA, Zhang B and White HS: **Nanoparticle transport in conical-shaped nanopores**. *Anal Chem* 2011, **83**:3840-7. | Article | PubMed
41. Dekker C: **Solid-state nanopores**. *Nat Nanotechnol* 2007, **2**:209-15. | Article | PubMed
42. Ito T, Sun L, Henriquez RR and Crooks RM: **A carbon nanotube-based coulter nanoparticle counter**. *Acc Chem Res* 2004, **37**:937-45. | Article | PubMed
43. Henriquez RR, Ito T, Sun L and Crooks RM: **The resurgence of Coulter counting for analyzing nanoscale objects**. *Analyst* 2004, **129**:478-82. | Article | PubMed
44. Vogel R, Willmott G, Kozak D, Roberts GS, Anderson W, Groenewegen L, Glossop B, Barnett A, Turner A and Trau M: **Quantitative sizing of nano/microparticles with a tunable elastomeric pore sensor**. *Anal Chem* 2011, **83**:3499-506. | Article | PubMed
45. Sun L and Crooks RM: Single Carbon Nanotube Membranes: **A Well-Defined Model for Studying Mass Transport through Nanoporous Materials**. *Journal of the American Chemical Society* 2000, **122**(49):12340-12345. | Article
46. Kozak D, Anderson W, Vogel R and Trau M: **Advances in Resistive Pulse Sensors: Devices bridging the void between molecular and microscopic detection**. *Nano Today* 2011, **6**:531-545. | Article | PubMed Abstract | PubMed Full Text
47. Willmott GR, Vogel R, Yu SS, Groenewegen LG, Roberts GS, Kozak D, Anderson W and Trau M: **Use of tunable nanopore blockade rates to investigate colloidal dispersions**. *J Phys Condens Matter* 2010, **22**:454116. | Article | PubMed
48. Sexton LT, Horne LP and Martin CR: **Developing synthetic conical nanopores for biosensing applications**. *Mol Biosyst* 2007, **3**:667-85. | Article | PubMed
49. Willmott GR, Broom MF, Jansen ML, Young RM, & Arnold WM: **Tunable Elastomeric Nanopore**. *Molecular and nano-tubes* 2011, pp:209-262. | Book
50. Vogel R, Willmott G, Kozak D, Roberts GS, Anderson W, Groenewegen L, Glossop B, Barnett A, Turner A and Trau M: **Quantitative sizing of nano/microparticles with a tunable elastomeric pore sensor**. *Anal Chem* 2011, **83**:3499-506. | Article | PubMed
51. Vogel R, Anderson W, Eldridge J. E, Glossop B and Willmott G. R: **A Variable Pressure Method for Characterising Nanoparticle Surface Charge using Pore Sensors**. *Anal. Chem* 2012, **84**:3125-3132. | Article
52. Roberts GS, Yu S, Zeng Q, Chan LC, Anderson W, Colby AH, Grinstaff MW, Reid S and Vogel R: **Tunable pores for measuring concentrations of synthetic and biological nanoparticle dispersions**. *Biosens Bioelectron* 2012, **31**:17-25. | Article | PubMed
53. Sowerby SJ, Broom MF and Petersen GB: **Dynamically resizable nanometre-scale apertures for molecular sensing**. *Sensors and Actuators B: Chemical* 2007, **123**(1):325-330. | Article
54. Michelle Low, Sam Yu, Ming Yong Han, Xiaodi Su: **Investigative Study of Nucleic Acids-Gold Nanoparticles Interactions Using Laser-based Techniques, Electron Microscopy and Resistive Pulse Sensing with a Nanopore.** *Australian Journal of Chemistry 2011,* **64**:1229-1234. | Article
55. Roberts GS, Kozak D, Anderson W, Broom MF, Vogel R and Trau M: **Tunable nano/micropores for particle detection and discrimination: scanning ion occlusion spectroscopy**. *Small* 2010, **6**:2653-8. | Article | PubMed
56. Willmott GR, Platt M, & Lee GU: **Resistive pulse sensing of magnetic beads and supraparticle structures using tunable pores**. *Biomicrofluidics* article 2012, **6:**014103. | Article
57. Ang YS and Yung LY: **Rapid and label-free single-nucleotide discrimination via an integrative nanoparticle-nanopore approach**. *ACS Nano* 2012, **6**:8815-23. | Article | PubMed
58. Willmott GR & Parry BET: **Resistive pulse asymmetry for nanospheres passing through tunable submicron pores**. *Journal of Applied Physics* 2011, **109**(9):094307. | Article
59. **1-Step™ ABTS**. | Pdf
60. Cohen-Tannoudji L, Bertrand E, Baudry J, Robic C, Goubault C, Pellissier M, Johner A, Thalmann F, Lee NK, Marques CM and Bibette J: **Measuring the kinetics of biomolecular recognition with magnetic colloids**. *Phys Rev Lett* 2008, **100**:108301. | Article | PubMed
61. Perry RW, Meng G, Dimiduk TG, Fung J and Manoharan VN: **Real-space studies of the structure and dynamics of self-assembled colloidal clusters**. *Faraday Discussions* 2012, **159:**211-234. | Article
62. Gasser U, Weeks ER, Schofield A, Pusey PN and Weitz DA: **Real-space imaging of nucleation and growth in colloidal crystallization**. *Science* 2001, **292**:258-62. | Article | PubMed
63. Savage JR and Dinsmore AD: **Experimental evidence for two-step nucleation in colloidal crystallization**. *Phys Rev Lett* 2009, **102**:198302. | Article | PubMed

Citation:
Billinge ER, Muzard J and Platt M: **Tunable resistive pulse sensing as a tool to monitor analyte induced particle aggregation**. *Nanomater Nanosci* 2013, **1**:1.
http://dx.doi.org/10.7243/2053-0927-1-1